Exchange and spin-orbit induced phenomena in diluted (Ga,Mn)As from first principles

J. Kudrnovský and V. Drchal
Institute of Physics, Academy of Sciences of the Czech Republic, Na Slovance 2, CZ-182 21 Praha 8, Czech Republic

I. Turek
Institute of Physics of Materials, Academy of Sciences of the Czech Republic, Žižkova 22, CZ-616 62 Brno, Czech Republic
(Received 14 June 2016; published 26 August 2016)

Physical properties induced by exchange interactions (Curie temperature and spin stiffness) and spin-orbit coupling (anomalous Hall effect, anisotropic magnetoresistance, and Gilbert damping) in the diluted (Ga,Mn)As ferromagnetic semiconductor are studied from first principles. Recently developed Kubo-Bastin transport theory and nonlocal torque operator formulation of the Gilbert damping as formulated in the tight-binding linear muffin-tin orbital method are used. The first-principles Liechtenstein mapping is employed to construct an effective Heisenberg Hamiltonian and to estimate Curie temperature and spin stiffness in the real-space random-phase approximation. Good agreement of calculated physical quantities with experiments on well-annealed samples containing only a small amount of compensating defects is obtained.

DOI: 10.1103/PhysRevB.94.054428

I. INTRODUCTION

Diluted ferromagnetic semiconductors are interesting materials as they allow one to control both the carrier concentration and magnetic state of the system. A prototypical example of such systems is the diluted magnetic semiconductor (DMS) (Ga,Mn)As. Its magnetic and transport properties were intensively studied theoretically more than a decade ago using the empirical J_{pd} model (see Ref. [1] for extensive review on the subject).

Despite the fact that original high expectations for technological applications of (Ga,Mn)As in the spintronics have not been met, mostly due to the low Curie temperature well below room temperature, an effort to gain detailed understanding of its physical properties, in particular those driven by spin-orbit coupling, continues. One of the reasons is the technological progress in preparation of well-defined samples containing a low concentration of compensating defects (As[Ga] antisites and Mn interstitials) [2,3]. This opens the way for a detailed comparison of experiment with first-principles simulations which was difficult on samples with unknown compensation, mainly as concerns transport studies. In particular, in a recent first-principles review on the subject of DMS [4] spin-orbit driven phenomena are completely missing.

In this study we wish therefore to concentrate on the first-principles simulation of spin-orbit driven phenomena such as the anisotropic magnetoresistance (AMR), anomalous Hall conductivity (AHC), and the Gilbert damping (GD). Experimentally closely related to the determination of the GD is the measurement of the spin stiffness (D_{stiff}) and the Curie temperature (T_{c}) [2]. We therefore calculate also these quantities related to exchange interactions. We wish to study a broad range of independent physical properties of a given material within the framework of the unified electronic structure model. Such study will allow not only for their deeper understanding, but also help to reveal strong and weak points of first-principles simulations on one side, and also to judge on the quality of sample preparation on the other side.

We shall concentrate on the GaAs doped with substitutional Mn atoms on the Ga sublattice, where the comparison between theory and experiment is the most straightforward. However, we will present also chosen results for alloys containing compensating defects such as As antisites and Mn interstitials. A detailed comparison of recent experimental studies [2,3,5] with the results of present simulations is the main aim of the present study.

II. FORMALISM

The electronic structure calculations are performed in the framework of the Green function formulation of the fully relativistic (Dirac) tight-binding linear muffin-tin orbital (TB-LMTO) method and the local spin-density approximation. The effect of impurities is included in the framework of the coherent potential approximation (CPA) [6]. The empty spheres are included into the zincblende lattice for a good space filling. The zincblende lattice thus formally consists of four interpenetrating fcc sublattices A-B-C-D aligned along the [111] direction and occupied, respectively, as Ga-As-E1-E2. Here, E1 and E2 denote different empty spheres with four As and Ga nearest neighbors (NN), respectively. The calculations employ the s,p,d basis, the same atomic radii for all atoms, and the Vosko-Wilk-Nusair exchange-correlation potential [7]. The Ga $3d$ states are treated as core states giving the bandwidth and gap of ideal GaAs close to the experimental values. Finally, the scalar-relativistic TB-LMTO codes are used to construct the effective isotropic Heisenberg Hamiltonian from which T_{c} and D_{stiff} are determined. It should be noted that there exist theories, both model [8] and the first-principles [9] ones, in which the effect of spin-orbit coupling on exchange interactions is considered. A detailed study of such effect is beyond the scope of the present paper. We just mention that the effect of spin-orbit coupling on the isotropic exchange interactions, relevant for determination of T_{c} and D_{stiff}, was found to be weak for DMSs [9].

The Mn atoms in the substitutional position (Mn_s) on the Ga sublattice which act as a single acceptor are the dominating defect in well-annealed samples. There are two possible compensating native defects: (i) As antisites on the Ga sublattice ($\mathrm{As}_{\mathrm{Ga}}$), and (ii) Mn interstitials (Mn_i) and

one cannot exclude their common presence in the sample. As_{Ga} and Mn_i act ideally as double donors. They both reduce the carrier concentration and the latter one also the effective concentration of magnetically active atoms because of possible formation of the Mn_s-Mn_i pair (see, e.g., Ref. [10]) which acts as a magnetically inactive object due to the opposite moments of Mn_s and Mn_i. Such a dimer can also remove less than two holes, a problem which is not yet clearly resolved. Although there exists some way to overcome this problem approximately, e.g., for the estimate of T_c [11], related study of corresponding transport properties for such a case is beyond the scope of this paper and in the present study we will assume ideal uncorrelated Mn substitutionals and Mn interstitials. In agreement with the experiment [12] we will assume that Mn_i occupies a tetrahedral position (E1) with As as the nearest neighbors.

The effective exchange interactions between Mn atoms for a given shell s, J_s, are determined by the Liechtenstein mapping procedure [13] generalized to random ferromagnets [14,15]. It is now established that both the Curie temperature [16–18] and spin stiffness [19] can be influenced by the percolation effects in systems with low concentration of magnetic atoms. We shall use the real-space random-phase approximation (RPA) with random distribution of moments in the simulation cell for both T_c [18] and D_{stiff} [19]. Robust results for both T_c and D_{stiff} were obtained for simulation cells with periodic boundary conditions containing about 4000 Mn moments averaged over 50 random configurations.

The conductivity tensor is evaluated using a recent Kubo-Bastin formulation of the fully relativistic transport in disordered magnetic alloys which includes both the Fermi-surface and Fermi-sea terms on equal footing [20]. It should be noted that the Fermi-sea term was mostly neglected in previous AHC studies and we wish to verify here how important it is for (Ga,Mn)As alloy. The disorder-induced vertex corrections are included in the CPA [21]. Their inclusion is simplified by the present formulation of the velocity as the intersite hopping [22] which leads to nonrandom velocity matrices. Once the conductivity tensor $\sigma_{\mu\nu}$ $(\mu,\nu = x,y,z)$ is determined, the AMR and AHC are found from its components. Assuming the magnetization pointing along the z axis, we have

$$\mathrm{AMR} = -(\sigma_{zz} - \sigma_{xx})/\sigma_{\mathrm{tot}}, \quad \mathrm{AHC} = \sigma_{xy}, \tag{1}$$

where $\sigma_{\mathrm{tot}} = (2\sigma_{xx} + \sigma_{zz})/3$. Large number of k points (of order 10^8 in the full Brillouin zone) is needed for well-converged results. We refer the reader to a recent paper [20] for details.

The GD constant is an important phenomenological parameter describing the magnetization dynamics. It is evaluated here with the help of a recently developed approach using nonlocal torques as an alternative to the usual local torque operators entering the torque-correlation formula [23]. This leads to effective torques which are represented as non-site-diagonal and spin-independent matrices which again simplifies evaluation of disorder-induced vertex corrections. It should be noted that vertex corrections play an essential role in the present formulation and their neglect leads to quantitatively and physically incorrect results [23]. Our formulation gives results which compare well to other first-principles studies [24–26]. In this study we will concentrate on the GD due to chemical disorder introduced by Mn impurities/As antisites. It should be noted that there are other sources of damping, e.g., the temperature effects due to phonons and spin fluctuations [27,28]. In chosen cases, we will discuss briefly the effect of spin fluctuations on results using the uncompensated disordered local moment (uDLM) approach [29,30].

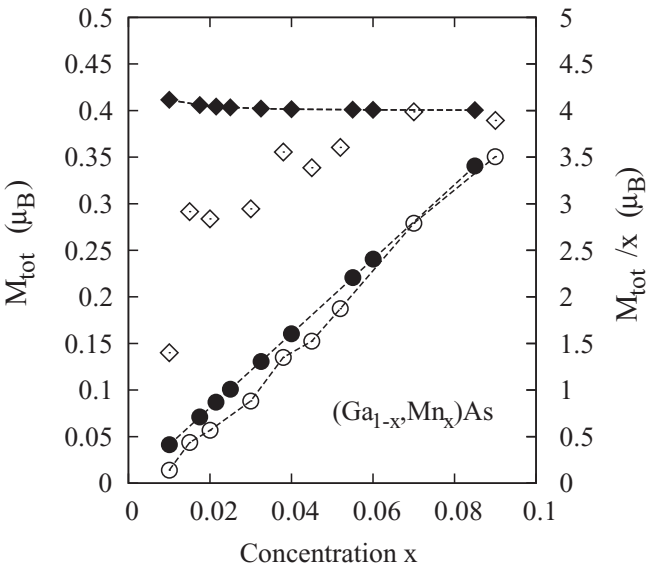

FIG. 1. The total magnetic moments in μ_B as a function of the Mn concentration x in $(Ga_{1-x},Mn_x)As$ alloys. (Left scale) Calculated magnetic moments (solid circles) and experiment [2] (open circles). (Right scale) Calculated values per Mn atom (solid diamonds) and experimental values [2] (open diamonds).

III. RESULTS AND DISCUSSION

A. Electronic structure: Mn impurities

The scalar-relativistic electronic structure of (Ga,Mn)As is well documented in the literature (see, e.g., Ref. [4]) and we will not reiterate it here. We have verified that the spin-orbit coupling influences magnetic moments only weakly. We present in Fig. 1 calculated relativistic total spin moments as a function of the Mn concentration x and compare them with available experimental data [2]. Corresponding orbital moments are very small, varying from negative value -0.0003 μ_B for $x = 0.01$ to positive one $+0.0007$ μ_B for $x = 0.085$. The calculated linear dependence of the total moment on Mn doping agrees reasonably well with experiment [2] and, in turn, indicates well-annealed samples with a low content of compensating defects. Such linear dependence also reflects the fact that each Mn atom contributes by 4 μ_B to the total moment (half-metallic state). We have therefore plotted the concentration dependence of the total moment per Mn atom. This quantity is very close to 4 μ_B in the theory as expected. On the other hand, despite the above-mentioned good agreement between calculated and measured total moments, the experimental values per Mn atom do not agree so well, in particular for low Mn concentrations. This is partly due to the large enhancement factor (e.g., 100 for $x = 0.01$), but it also indicates violation of a simple rule that each Mn spin contributes by 4 μ_B. In different words, in spite

TABLE I. Local Mn moments (m_t^{Mn}), total moments (M_{tot}), and total moments per Mn atom (M_{tot}/Mn) (in μ_{B}) for GaAs doped with Mn atoms in the substitutional position ($t = s$) without and with As[Ga] antisites or with the interstitial atom ($t = i$) in position with four nearest-neighbor As atoms. Shown are spin and orbital (in brackets) moments for three different models A, B, and C. Models B and C represent compensated samples with the same nominal Mn concentration $x^{\mathrm{Mn}} = 0.055$.

Model	x_s^{Mn}	$y_{\mathrm{Ga}}^{\mathrm{As}}$	x_i^{Mn}	m_s^{Mn}	m_i^{Mn}	M_{tot}	M_{tot}/Mn
(A)	0.055	0.0	0.0	3.71 (0.03)	–	0.221	4.00 (0.003)
(B)	0.055	0.01	0.0	3.82 (0.03)	–	0.240	4.37 (0.005)
(C)	0.04	0.0	0.015	3.88 (0.03)	−3.37 (−0.05)	0.115	2.09 (−0.007)

of good annealing, the native defects are still present and their content differs slightly in different samples. We mention this fact because, e.g., the GD is inversely proportional to the total spin moment and this can be one of the reasons why the experimental values are larger than the theoretical ones, in particular for low x (see Sec. III D). We also mention that the local Mn moment depends very weakly on the Mn concentration being about 3.7 μ_{B}.

A systematic study of the effect of compensating defects is beyond the scope of this paper, we nevertheless compare in Table I magnetic moments for three typical models with the same nominal concentration of Mn atoms: (i) All Mn atoms are substitutional (model A), (ii) the same as in the previous case, but with compensating As[Ga] antisites (model B), and (iii) a part of nominal Mn atoms is in the interstitial position with four As NN (model C). The latter two cases are compensated alloys and both defects act ideally as double donors. We have chosen an interstitial site that is observed in the experiment [12], but the results for the interstitial site with four Ga NN are very similar. The half-metallic character of the alloy is found for the substitutional case while the total moment is enhanced/reduced in a compensated case with As antisites/Mn interstitials, respectively. The total moment per Mn atom increases with the addition of As antisites and it becomes 5 μ_{B} for the fully compensated case (if $y_{\mathrm{Ga}}^{\mathrm{As}} = x^{\mathrm{Mn}}/2$). This is due to a gradual filling of empty states in the valence majority band due to the donorlike As[Ga] antisites. The reduction of the total moment for the Mn interstitial is due to the antiparallel orientation of moments of the Mn substitutional and interstitial atoms. In agreement with a total energy supercell study [31] we have obtained that both interstitial positions have very similar energies for a model without Mn substitutionals (the site with four Ga NN is the ground state). The presence of Mn substitutionals reverses the situation and the theoretically predicted ground state (site with four As NN) agrees with the experiment [12]. It should be noted, however, that this agreement should not be overemphasized as the CPA treats Mn_s and Mn_i as uncorrelated defects which is not probably the case when Mn_s-Mn_i dimers [10] are formed and the energetics thus could be influenced. The reason is that a correlated pair has the total moment close to zero and it is thus magnetically inactive, the fact which was used for the estimation of T_{c} in compensated samples [11]. It is obvious that such a situation can influence quantities explicitly depending on magnetic moments like, e.g., T_{c}, AHC, and GD. It should be mentioned that the total moment can be reduced also by the spin disorder at finite temperatures. The existence of spin disorder induced by the As antisites even at the zero temperature was predicted in Ref. [32].

It should be also noted that the theory assumes an ideal Mn substitution, namely, the fact that one Mn atom releases one hole. The dependence of the hole concentration p on the Mn doping should be thus linear. It is seen, however, that even in well-annealed samples [2] the dependence with a variable slope is observed indicating the existence of a certain amount of Mn interstitials for higher doping [1,33]. This fact has to be kept in mind for a detailed comparison of the theory and experiment, in particular for transport properties. Finally, we also note that the above-mentioned strong variation of the carrier concentration induced by small concentration changes is one of the most important features which distinguishes the behavior of magnetic impurities in a nonmagnetic metal and a semiconductor. Such difference is particularly important for transport properties which depend sensitively on the carrier concentration so that the experience from metals related, e.g., to AHC [34] or GD [26], may not be directly applicable in the DMSs.

B. Curie temperature and spin stiffness

We have performed calculations of T_{c} and D_{stiff} in the framework of the RPA including the percolation effects [18,19] and compared them in Fig. 2 with the experiment [2]. We have employed exchange integrals up to the distance 6.36 a, or 229 shells (a is the lattice constant). Previous simulations [18,19] used up to 62 shells, or distance up to 4.0 a, but they agree reasonably well. We note also a good agreement with T_{c} values estimated by the Monte Carlo method which takes into account random spin distribution in the sample [4,16,17].

We have found overall good agreement between the calculated and measured values of T_{c} and D_{stiff} for well-annealed samples [2] and a weak concentration dependence of D_{stiff}. A good agreement with another experimental data [5] for T_{c} was also obtained. We mention the effect of the magnetic percolation, in particular for low Mn concentrations. For example, the mean-field values of T_{c} are almost four times larger for $(\mathrm{Ga}_{0.98},\mathrm{Mn}_{0.02})\mathrm{As}$ and two times larger for $(\mathrm{Ga}_{0.91},\mathrm{Mn}_{0.09})\mathrm{As}$ than the present ones estimated in the RPA approach with percolation effects included. It should be noted that compensating defects can reduce the experimental and calculated T_{c} non-negligibly [11].

As concerns evaluation of D_{stiff}, one should mention a recent extensive theoretical study of the spin-wave spectra of (Ga,Mn)As in the framework of the pd Zener model and the $spds^*$ tight-binding approximation [8]. We just mention that theoretical estimates of D_{stiff} are found in the range 100–230 meV Å^2 for concentrations studied in the present

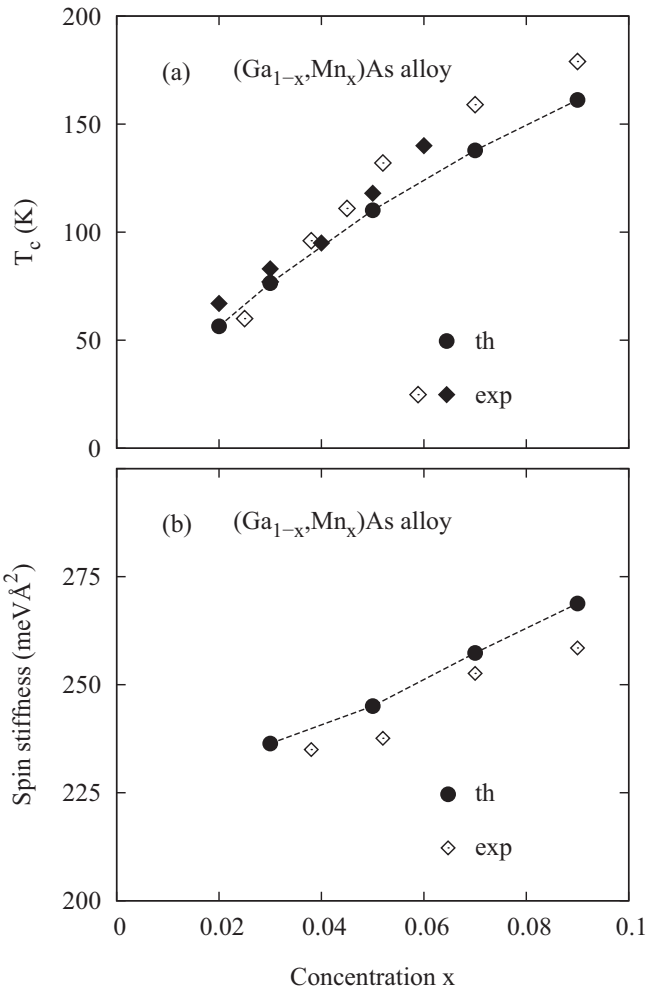

FIG. 2. Calculated (solid circles) and experimental (open diamonds [2] and solid diamonds [5]) values of the Curie temperature (a) and the spin stiffness (b) plotted as a function of the concentration x in $(Ga_{1-x},Mn_x)As$ alloys. The RPA approach which includes percolation effects for random spins in the simulation cell is employed.

paper, but their concentration dependence exhibits a larger slope and smaller values as compared to the present study.

C. Transport properties: conductivity, AMR, and AHC

1. Isotropic conductivity

We shall start the study of transport properties with discussion of the conductivity σ_{tot} for $(Ga_{1-x},Mn_x)As$ with different Mn concentrations. Results of calculations are compared with corresponding experimental values [2,5] in Fig. 3. Calculated σ_{tot} values increase with impurity Mn concentration indicating a nonmetallic behavior. Such behavior is a result of two opposite trends, namely, a decrease of σ_{tot} with impurity concentration and its increase due to the increase of the hole carrier concentration p with Mn doping (one Mn atom adds ideally one hole into the valence band). A net effect is the observed increase of σ_{tot}. Two sets of experimental values follow closely the trend of calculated ones, but they are systematically smaller, although those of Ref. [5] show

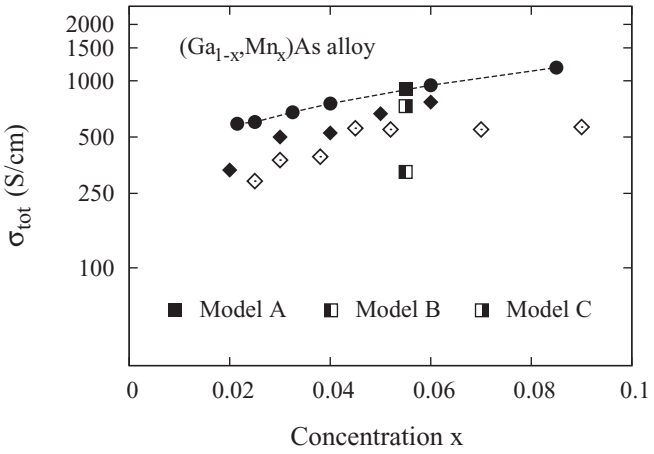

FIG. 3. Calculated σ_{tot} in the logarithmic scale (solid circles) for $(Ga_{1-x},Mn_x)As$ as a function of the Mn concentration x is compared with experimental data [2] (open diamonds) and [5] (solid diamonds). The conductivities corresponding to compensating defects (the models A, B, and C in Table I) are shown by various square symbols.

a slightly better agreement. This indicates a presence of some additional (compensating) defects which will lower conductivity, either by increasing scatterings on additional defects or by reducing the sample carrier concentration p (donor defects). It should be noted that the mean-field theory combined with a Born approximation description of impurity scattering in the framework of the Boltzmann equation and assuming only substitutional defects [3,35] overestimates experimental values of σ_{tot} few times. A systematic study of the effect of compensating defects on σ_{tot} is beyond the scope of the paper; we just show a typical effect of Mn interstitials and As antisites for models with the same nominal Mn concentration which were already mentioned above in Table I. It is clearly seen that compensating defects reduce calculated σ_{tot} values and their inclusion will further improve the agreement between theory and experiment.

2. Anomalous Hall effect

Calculated AHC values (σ_{xy}) are compared in Fig. 4 with two different experimental results [5,36]. It should be noted that in the experiment [5] there is an apparent deficit of holes for $x = 0.08$ indicating a not well-annealed sample. Calculations predict, in accord with the experiment, an increase of σ_{xy} with Mn doping with σ_{xy} values being in the range of 10 S/cm to 30 S/cm. Experimental values of σ_{xy} are estimated from measured values of ρ_{xy} and ρ_{tot} using the expression,

$$\sigma_{xy} = -\rho_{xy}/\rho_{tot}^2 = -\rho_{xy}\,\sigma_{tot}^2. \quad (2)$$

From the experimentally measured resistance and the film thickness one can extract the sample resistivity. Due to annealing and possible oxidation defects segregate close to the surface making the exact value of the effective film thickness, needed for the estimate of the resistivity, somehow uncertain. These facts have to be taken into account when comparing with the experimental data.

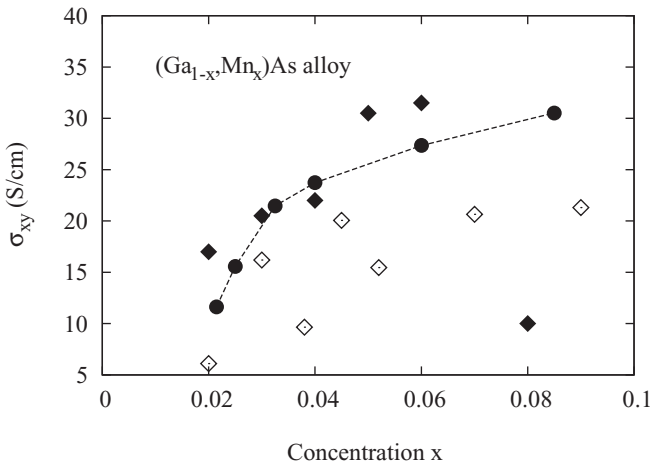

FIG. 4. Calculated AHC σ_{xy} (solid circles) as a function of the Mn concentration for $(Ga_{1-x},Mn_x)As$ are compared with results of two experiments: Ref. [5] (solid diamonds) and Ref. [36] (open diamonds).

It is also clear that possible errors in σ_{tot} as seen, e.g., in Fig. 3, can influence values of thus estimated ρ_{tot} for different concentrations. We therefore show in Fig. 5 calculated and experimental values [5,36] of ρ_{xy}. We note that theoretical values are found in the range 20–45 $\mu\Omega$ cm while experimental ones are found in the range 60–105 $\mu\Omega$ cm. Also, with the exception of very low concentrations, absolute values of ρ_{xy} decrease with increasing Mn doping in agreement with the increase of σ_{xy} values. There is a disagreement between theory and experiment for very low Mn doping both for ρ_{xy} and σ_{tot} for reasons explained above. However, calculated and measured σ_{xy} show an acceptable agreement when determined using Eq. (2). One thus should be careful not to overestimate an agreement between the experiment and calculated σ_{xy} values obtained directly using simplified models (e.g., the virtual-crystal approximation) for systems with disorder without comparison of calculated values of the isotropic conductivity/resistivity. In other words, a correct theory should provide reasonable values for the whole conductivity tensor.

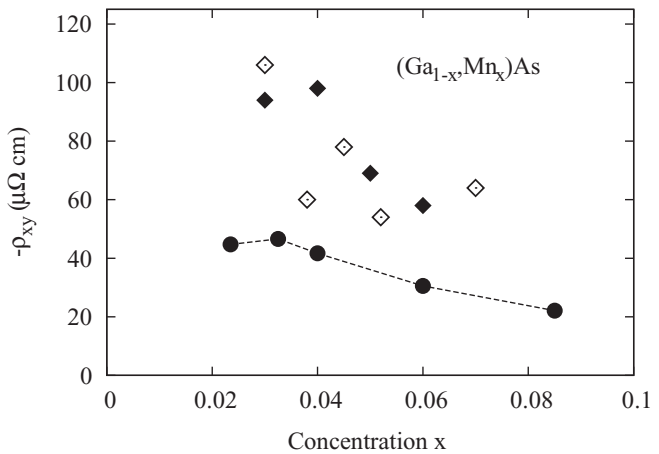

FIG. 5. The calculated values of ρ_{xy} (solid circles) and corresponding experimental results, Ref. [5] (solid diamonds) and Ref. [36] (open diamonds). Note the opposite sign of ρ_{xy}.

Smaller calculated values of ρ_{xy} are clearly due to the neglect of compensating defects present even in well-annealed samples. The effect of compensating defects is illustrated in Table II for a few cases, but again there is no attempt for a systematic study. We have tried to compare some typical cases, namely, alloys with Mn substitutionals only (Models 1 and 2), models containing also some amount of As[Ga] antisites (Models 3 and 4), models in which some part of Mn atoms is on interstitial sites (Models 5–7), and one model in which all possible defects are present (Model 8). The following conclusions can be made: (i) Additional disorder due to As antisites reduces σ_{tot} and brings calculated ρ_{xy} to a better agreement with the experiment. On the other hand, σ_{xy} is influenced only weakly; (ii) Mn interstitials are very strong scattering centers and increasing their concentration strongly reduces σ_{tot} and significantly increases ρ_{xy} while σ_{xy} changes only weakly; (iii) models with large content of compensating defects (Models 4, 6, and 7) have a small hole concentration p between 0.01 and 0.02; and (iv) Model 8 represents an alloy with all three defects present for which the Curie temperature and conductivity were obtained simultaneously in good agreement with the experiment [11,37].

Finally, we wish to discuss briefly some features of the AHC in DMS alloys. First, we omit the case of very low impurity concentrations which in metallic systems are dominated by skew scattering behavior for a few reasons. In the DMSs, there is a strong variation of the carrier number (holes) of the very low impurity concentration. Such behavior is quite different from that in metals, where the number of carriers is almost constant for low defect concentrations. Even more important is the fact that for very low Mn contents there is a transition between the regime of quasilocalized Mn levels (with a possible hopping transport regime) and the regime with the Mn impurity band merged into the host valence band with a conventional conductive regime [38]. The present CPA description of disorder becomes inapplicable for very low concentrations because the percolation effects, both the magnetic and transport ones, become important and influence transport properties. Second, we have impurity-induced vertex corrections to the Fermi-surface and Fermi-sea terms, nevertheless the latter ones are negligible. The importance of vertex corrections corresponding to the AHC depends on the alloy composition and the type of defects but they do not exceed 10%–15% of the total AHC.

3. Anisotropic magnetoresistance

We have included in Table II also the estimated AMR values [see Eq. (1)] for the above models. We have obtained negative, but very small AMR values in a broad concentration range for the case of only substitutional defects (Models 1 and 2). In particular, the AMR decreases from -0.185% to -0.039%. for $x \in (0.025, 0.085)$. A recent experiment [3] gives negative AMR values of order 1%–2% for very low Mn concentrations (x smaller than about 2.5%) and of order -0.25% to -0.5% for higher concentrations. It should be noted that much larger values of the AMR ratio were obtained in older measurements [35]. The AMR values ranging from -0.23% to -1.606% were calculated for various compensated samples and fall into the range found in the experiment [3]. A general feature of all

TABLE II. Total conductivity ($\sigma_{\rm tot}$) and σ_{xy} in S/cm, related total resistivity ($\rho_{\rm tot}$) and ρ_{xy} in $\mu\Omega$ cm, and the AMR ratio for various models. Here $x_t^{\rm Mn}$, $t = s,i$, and $y_{\rm Ga}^{\rm As}$ denote concentrations of Mn substitutional (s) and interstitial (i) atoms, and of As[Ga] antisites, respectively, for various models (Models 1–8).

Model	$x_s^{\rm Mn}$	$y_{\rm Ga}^{\rm As}$	$x_i^{\rm Mn}$	$\sigma_{\rm tot}$ (S/cm)	σ_{xy} (S/cm)	$\rho_{\rm tot}$ ($\mu\Omega$ cm)	ρ_{xy} ($\mu\Omega$ cm)	AMR (%)
(1)	0.04	0.0	0.0	754.7	23.72	1324	−41.65	−0.095
(2)	0.06	0.0	0.0	946.6	27.35	1056	−30.53	−0.066
(3)	0.055	0.01	0.0	732.2	27.82	1364	−52.02	−0.452
(4)	0.06	0.02	0.0	570.0	28.83	1752	−89.30	−1.063
(5)	0.05	0.0	0.005	742.5	25.12	1346	−45.61	−0.231
(6)	0.045	0.0	0.01	561.3	24.08	1779	−76.67	−0.589
(7)	0.06	0.0	0.025	314.6	20.49	3196	−208.93	−1.606
(8)	0.055	0.005	0.015	424.0	24.02	2353	−134.60	−1.195

samples with calculated AMR of order −1% is relatively high compensation (or low p values of order 0.01 to 0.02). In particular, a clear trend is seen by comparing Models 5–7: The decrease of the hole concentration p leads to larger AMR ratios.

D. Gilbert damping

The calculated dimensionless GD constants α for $(Ga_{1-x},Mn_x)As$ as a function of the Mn doping are compared with the experiment [2] in Fig. 6 (measurements were performed at 15 K). Experimental concentration dependence of the GD on Mn doping is well reproduced by present calculations, but theoretical values are smaller, in particular for very small x. In Refs. [26,39] a close relation between the concentration dependence of the density of states at the Fermi energy, DOS($E_{\rm F}$), and the dependence of the GD for the case of bcc-(Fe_{1-x},Co_x) alloys was illustrated.

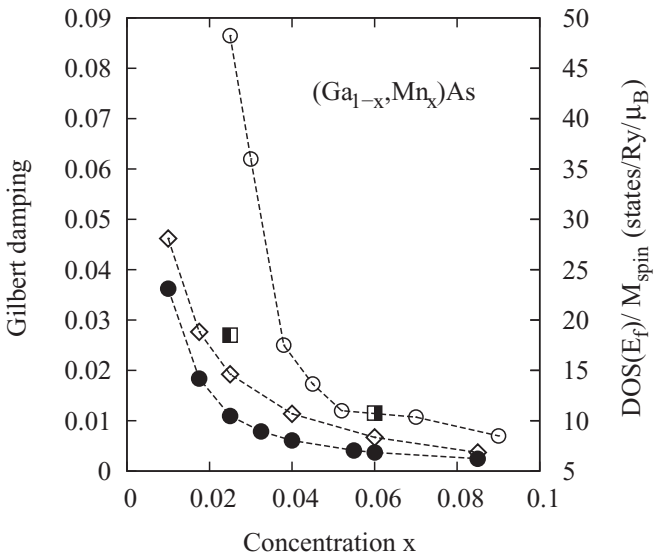

FIG. 6. (Left scale) The calculated Gilbert damping constants α (solid circles) as a function of the Mn concentration x in $(Ga_{1-x},Mn_x)As$ alloys. Half-filled square symbols show values for 10% of spins with reversed orientation at $x = 0.025$ and $x = 0.06$ calculated in the framework of the uDLM approach (see the text). The experimental values [2] (open circles) are also shown for comparison. (Right scale) The ratio DOS($E_{\rm F}$)/$M_{\rm spin}$ of the density of states at the Fermi energy to the total spin magnetic moment (diamonds) is shown as a function of x.

A similarly good agreement was found [23] also for ordering $L1_0$-FePt alloys as a function of the long-range order parameter. The DMS differ from the above transition metal alloys by a pronounced dependence of the magnetic moment M on the Mn concentration on which the GD depends inversely proportionally [23,26]. We have found that the quantity DOS($E_{\rm F}$)/M describes very well the concentration trend of the GD in $(Ga_{1-x},Mn_x)As$ alloys while DOS($E_{\rm F}$) itself does not.

There are two possible reasons for underestimation of calculated GD values as compared to the experiment. We know from Fig. 1 that experimental values of M are smaller as compared to theoretical ones so that changes in GD constants α proportional to M^{-1} may be non-negligible. Another source of possible enhancement of theoretical values is the presence of the spin disorder induced by temperature or by the As antisites [32]. The cases with 10% of spins with reversed orientations are shown for $x = 0.025$ and $x = 0.06$ by half-filled squares giving enhancement approximately by a factor of three. It should be noted that the present theory includes only damping due to the disorder and other possible sources are neglected, e.g., the extrinsic contribution due to the magnon scattering, thin film character of samples, etc.

Finally, the presence of compensating defects in the sample can also influence the calculated GD. The systematic study is beyond the scope of the paper; we just show in Table III the effect of As antisites and Mn interstitials for the reference $(Ga_{0.94},Mn_{0.06})As$ alloy. Addition of As antisites

TABLE III. Calculated Gilbert damping parameters α in the reference $(Ga_{0.94},Mn_{0.06})As$ alloy (ref) for different compensating defects, namely (i) As antisites on Ga sublattice (As_{Ga}), and (ii) Mn interstitials (Mn_i). In a separate column we also show the total spin moment $M_{\rm tot}$ for each model (in $\mu_{\rm B}$).

Model	$y_{\rm Ga}^{\rm As}$	$x_i^{\rm Mn}$	α	$M_{\rm tot}$
ref	0.0	0.0	0.00369	0.240
	0.005	0.0	0.00350	0.250
As_{Ga}	0.01	0.0	0.00334	0.260
	0.02	0.0	0.00316	0.280
	0.0	0.005	0.00423	0.225
Mn_i	0.0	0.020	0.00457	0.180
	0.0	0.025	0.00435	0.165

increases M_{tot} while Mn interstitials reduce it. There are thus two effects which influence the resulting value of the GD parameter for alloys with compensating defects: (i) The value of the total magnetic moment M_{tot} on which GD depends inversely proportionally, and (ii) an additional disorder due to compensating defects. The disorder due to As antisites is weak (the *sp* disorder) as contrasted with strong disorder due to Mn interstitials. A weak decrease of the GD parameter with an increase of As-antisite concentration can be thus understood as primarily due to an increase of M_{tot} while a weak disorder does not influence it. On the contrary, the GD parameter first increases with increasing concentration of Mn interstitials (which reduces M_{tot}) but increasing additional strong substitutional disorder acts in an opposite way: The GD parameter saturates and even starts to decrease for large interstitial concentration.

IV. CONCLUSIONS

We have presented the first-principles estimate of a broad range of physical quantities related to (Ga,Mn)As alloys based on a unified electronic structure model. We used the relativistic TB-LMTO-CPA approach to include spin-orbit effects and disorder and the mapping of the magnetic part of the total energy to the Heisenberg model to calculate concentration dependence of the Curie temperature and the spin stiffness which both include percolation effects. Calculations serve as inputs into the Kubo-Bastin linear response theory used to calculate the conductivity, the AHC, and the AMR values. Finally, the torque-correlation formalism based on nonlocal torques was used to estimate the Gilbert damping constant. All quantities were estimated from first principles. The main conclusions are following: (i) An overall good agreement of all calculated quantities with experiments on samples with low content of compensating defects was obtained; (ii) in some cases the agreement between theory and experiment is worse, but it could be improved by assuming the presence of compensating defects; (iii) disorder-induced vertex corrections to the AHC do not exceed 10%–15% of the total AHC in (Ga,Mn)As alloys. On the other hand, those corresponding to the Fermi-sea term are negligible; (iv) if the compensating defects are neglected, the AMR ratio has a correct sign, but its value is too small, but their correct description improves the quantitative agreement with the experiment; (v) calculated Gilbert damping parameter decreases with increasing concentration of Mn atoms. Its concentration trend is described very well by the empirical ratio $\mathrm{DOS}(E_{\mathrm{F}})/M$.

ACKNOWLEDGMENTS

The authors acknowledge financial support from the Czech Science Foundation (Grant No. 15-13436S) and they thank Prof. P. Němec, Dr. V. Novák, and Dr. K. Edmonds for kindly sending their data not shown in their papers, Refs. [2,5], and used here for comparison with calculated results.

[1] T. Jungwirth, J. Sinova, J. Mašek, J. Kučera, and A. H. MacDonald, Rev. Mod. Phys. **78**, 809 (2006).
[2] P. Němec, V. Novák, N. Tesařová, E. Rozkotová, H. Reichlová, D. Butkovičová, F. Trojánek, K. Olejník, P. Malý, R. P. Campion, B. L. Gallagher, J. Sinova, and T. Jungwirth, Nat. Commun. **4**, 1422 (2013).
[3] Z. Kašpar, K. Olejník, K. Výborný, H. Reichlová, M. Maryško, and V. Novák, Phys. Procedia **75**, 634 (2015).
[4] K. Sato, L. Bergqvist, J. Kudrnovský, P. H. Dederichs, O. Eriksson, I. Turek, B. Sanyal, G. Bouzerar, H. Katayama-Yoshida, V. A. Dinh, T. Fukushima, H. Kizaki, and R. Zeller, Rev. Mod. Phys. **82**, 1633 (2010).
[5] K. W. Edmonds, R. P. Campion, K.-Y. Wang, A. C. Neumann, B. L. Gallagher, C. T. Foxon, and P. C. Main, J. Appl. Phys. **93**, 6787 (2003), and a private communication.
[6] I. Turek, V. Drchal, J. Kudrnovský, M. Šob, and P. Weinberger, *Electronic Structure of Disordered Alloys, Surfaces and Interfaces* (Kluwer, Boston, 1997).
[7] S. H. Vosko, L. Wilk, and M. Nusair, Can. J. Phys. **58**, 1200 (1980).
[8] A. Werpachowska and T. Dietl, Phys. Rev. B **82**, 085204 (2010).
[9] H. Ebert and S. Mankovsky, Phys. Rev. B **79**, 045209 (2009).
[10] T. Dietl and H. Ohno, Rev. Mod. Phys. **86**, 187 (2014).
[11] G. Bouzerar, T. Ziman, and J. Kudrnovský, Phys. Rev. B **72**, 125207 (2005).
[12] L. M. C. Pereira, U. Wahl, S. Decoster, J. G. Correia, M. R. da Silva, A. Vantomme, and J. P. Araújo, Appl. Phys. Lett. **98**, 201905 (2011).
[13] A. I. Liechtenstein, M. I. Katsnelson, V. P. Antropov, and V. A. Gubanov, J. Magn. Magn. Mater. **67**, 65 (1987).
[14] J. Kudrnovský, I. Turek, V. Drchal, F. Máca, P. Weinberger, and P. Bruno, Phys. Rev. B **69**, 115208 (2004).
[15] I. Turek, J. Kudrnovský, V. Drchal, and P. Bruno, Philos. Mag. **86**, 1713 (2006).
[16] L. Bergqvist, O. Eriksson, J. Kudrnovský, V. Drchal, P. Korzhavyi, and I. Turek, Phys. Rev. Lett. **93**, 137202 (2004).
[17] K. Sato, W. Schweika, P. H. Dederichs, and H. Katayama-Yoshida, Phys. Rev. B **70**, 201202(R) (2004).
[18] G. Bouzerar, T. Ziman, and J. Kudrnovský, Europhys. Lett. **69**, 812 (2005).
[19] G. Bouzerar, Europhys. Lett. **79**, 57007 (2007).
[20] I. Turek, J. Kudrnovský, and V. Drchal, Phys. Rev. B **89**, 064405 (2014).
[21] K. Carva, I. Turek, J. Kudrnovský, and O. Bengone, Phys. Rev. B **73**, 144421 (2006).
[22] I. Turek, J. Kudrnovský, V. Drchal, L. Szunyogh, and P. Weinberger, Phys. Rev. B **65**, 125101 (2002).
[23] I. Turek, J. Kudrnovský, and V. Drchal, Phys. Rev. B **92**, 214407 (2015).
[24] A. A. Starikov, P. J. Kelly, A. Brataas, Y. Tserkovnyak, and G. E. W. Bauer, Phys. Rev. Lett. **105**, 236601 (2010).
[25] A. Sakuma, J. Phys. Soc. Jpn. **81**, 084701 (2012).
[26] S. Mankovsky, D. Ködderitzsch, G. Woltersdorf, and H. Ebert, Phys. Rev. B **87**, 014430 (2013).
[27] Y. Liu, A. A. Starikov, Z. Yuan, and P. J. Kelly, Phys. Rev. B **84**, 014412 (2011).

[28] H. Ebert, S. Mankovsky, K. Chadova, S. Polesya, J. Minár, and D. Ködderitzsch, Phys. Rev. B **91**, 165132 (2015).
[29] B. L. Gyorffy, A. J. Pindor, J. Staunton, G. M. Stocks, and H. Winter, J. Phys. F: Met. Phys. **15**, 1337 (1985).
[30] J. Kudrnovský, V. Drchal, S. Khmelevskyi, and I. Turek, Phys. Rev. B **84**, 214436 (2011).
[31] J. Mašek and F. Máca, Phys. Rev. B **69**, 165212 (2004).
[32] P. A. Korzhavyi, I. A. Abrikosov, E. A. Smirnova, L. Bergqvist, P. Mohn, R. Mathieu, P. Svedlindh, J. Sadowski, E. I. Isaev, Yu. Kh. Vekilov, and O. Eriksson, Phys. Rev. Lett. **88**, 187202 (2002).
[33] J. Mašek, I. Turek, J. Kudrnovský, F. Máca, and V. Drchal, Acta Phys. Pol. A **105**, 637 (2004).
[34] B. Zimmermann, K. Chadova, D. Ködderitzsch, S. Blügel, H. Ebert, D. V. Fedorov, N. H. Long, P. Mavropoulos, I. Mertig, Yu. Mokrousov, and M. Gradhand, Phys. Rev. B **90**, 220403(R) (2014).
[35] T. Jungwirth, J. Sinova, K. Y. Wang, K. W. Edmonds, R. P. Campion, B. L. Gallagher, C. T. Foxon, Q. Niu, and A. H. MacDonald, Appl. Phys. Lett. **83**, 320 (2003).
[36] V. Novák (private communication).
[37] J. Kudrnovský, G. Bouzerar, and I. Turek, Appl. Phys. Lett. **91**, 102509 (2007).
[38] J. Mašek, F. Máca, J. Kudrnovský, O. Makarovsky, L. Eaves, R. P. Campion, K. W. Edmonds, A. W. Rushforth, C. T. Foxon, B. L. Gallagher, V. Novák, J. Sinova, and T. Jungwirth, Phys. Rev. Lett. **105**, 227202 (2010).
[39] M. A. W. Schoen, D. Thonig, M. L. Schneider, T. J. Silva, H. T. Nembach, O. Eriksson, O. Karis, and J. M. Shaw, Nature Phys. (2016), doi:10.1038/nphys3770.